Challenge Journal of Structural Mechanics

Research Article

Structural behavior of ferrocement beams with circular openings

Yousry B. I. Shaheen [a], Zeinab A. Etman [a], Ahmed A. F. Mohamed [a,*]

[a] *Department of Civil Engineering, Menoufia University, 32511 Shebin ElKoum, Menofia, Egypt*

ABSTRACT

The construction sector is a major contributor to resource consumption and waste generation. Therefore, developing more efficient and sustainable materials and infrastructure is a top priority for achieving the Sustainable Development Goals. This research aims to contribute to this effort by studying the behavior of ferrocement beams with circular openings, with the goal of understanding their behavior under various loads and determining their potential use in designing more resilient and sustainable structures. Fifteen beams with different reinforcement mesh types were subjected to experimental testing under four-point loading, one group serves as the control with conventional reinforcement, while others vary in mesh type and opening configurations. All beams maintained approximately close reinforcement ratios, employing either two layers of welded galvanized steel mesh or a single layer of expanded steel mesh. Using numerical models, all fifteen beams were analyzed with the structural analysis program ANSYS V. 15 to study their non-linear shear behaviors and compare them with experimental data, focusing on load-deflection curves and failure modes. Results show that beams reinforced with expanded steel mesh achieved higher ultimate loads than those with welded mesh, with increases up to 81.59% depending on the opening configuration. However, beams with openings generally exhibited reduced ultimate loads, averaging 26.85% for welded mesh and 32.13% for expanded mesh, compared to beams without openings. Vertical openings, particularly with multiple openings, resulted in significant load decreases.

ARTICLE INFO

Article history:
Received 6 July 2024
Revised 2 September 2024
Accepted 12 September 2024

Keywords:
Ferrocement
Welded meshes
Expanded meshes
Numerical analysis
Circular openings
Optimizing material

1. Introduction

Ferrocement is a composite material consisting of a mortar matrix reinforced with multiple layers of steel mesh embedded within it (Shaheen and Essam 2017; Shaheen et al. 2023a; Hekal et al. 2024). Similar to reinforced concrete, it offers an effective solution for structural reinforcement due to its superior tensile strength, durability, and crack resistance. Developed in the 1940s by Italian architect P. L. Nervi, ferrocement is valued for its global material availability, ease of shaping, and cost-effectiveness, making it ideal for a wide range of structural elements, including walls, floors, and water-retaining structures. Composed primarily of cement, sand, and water, ferrocement can be enhanced with additives like pozzolanic materials (e.g., silica fume, fly ash) for improved performance.

In modern construction, there is an increasing focus on creating lightweight, high-quality, cost-effective, and environmentally friendly structures. Traditional concrete production generates significant waste, impacting the environment (Rashwan and Abourizk 1997). However, the use of recycled concrete can mitigate pollution and offer economic benefits (Abou-Zeid 2002).

Studies show that ferrocement is adaptable to increased loads, with reduced crack widths compared to reinforced concrete (Shaheen et al. 2011). The number of wire mesh layers (volume fraction) significantly impacts ferrocement's tensile strength, correlating with the initial cracking tensile strength based on reinforcement surface area (Shaheen and Hala 2017).

Shaheen et al. (2023b) studied the flexural behavior of ferrocement beams using fourteen beams, reinforced with either expanded or welded meshes, and measuring

* *Corresponding author*. Tel.: +20-100-854-3300 ; E-mail address: ahmedabdallahnebar000@gmail.com (A. A. F. Mohamed)
ISSN: 2149-8024 / DOI: https://doi.org/10.20528/cjsmec.2024.04.001

1000 mm by 100 mm by 150 mm. All beams were tested to failure under flexural loads. The study found that ferrocement beams exhibited notable ductility, high ultimate and serviceability loads, and crack resistance.

Previous research advocates for transverse openings in ferrocement beams for utility pipelines in contemporary construction. Structural elements in modern buildings frequently require openings for pipes or ducts. However, creating these openings in existing reinforced concrete beams disrupts the stress flow, which consequently reduces shear capacity and stiffness. Reduced stiffness may lead to excessive deflection under load, prompting significant redistribution of internal forces in the beam (Shaheen et al. 2022).

As the literature has been gone through, Limited research exists on the impact of circular openings on the behavior of ferrocement beams, emphasizing the need for this current study.

A finite element model is generated using ANSYS FEA and nonlinear (NL) analysis has been performed to simulate the behavior of tested specimens. The findings indicate that finite element simulations accurately approximate experimental results, providing valuable insights for future construction practices.

Overall, this research aims to fill a knowledge gap by studying the effects of circular openings on ferrocement beams, providing valuable insights for future design and construction practices. It contributes to sustainable construction by investigating the impact of circular openings on ferrocement beams, offering insights for designing more efficient and resilient structures, optimizing material use, and reducing environmental impact.

2. Research Methodology

The research methodology utilized in this study is represented through two comprehensive flowcharts that detail both the experimental and numerical approaches as shown in Fig.1. The first flowchart outlines the experimental procedure, beginning with the preparation of ferrocement beam specimens, including material selection, mixing, casting, and curing. It proceeds through the testing setup, involving instrumentation and load application, and concludes with data collection focusing on crack patterns, deflection, and load analysis. The second flowchart illustrates the numerical modeling process using finite element analysis (FEA) conducted via ANSYS V.15 software. This flowchart captures the stages of geometry modeling, load application, and boundary condition setup, followed by validation steps where numerical results are compared with experimental data to ensure accuracy. These flowcharts provide a clear and systematic overview of the research processes, facilitating a better understanding of the methodologies employed.

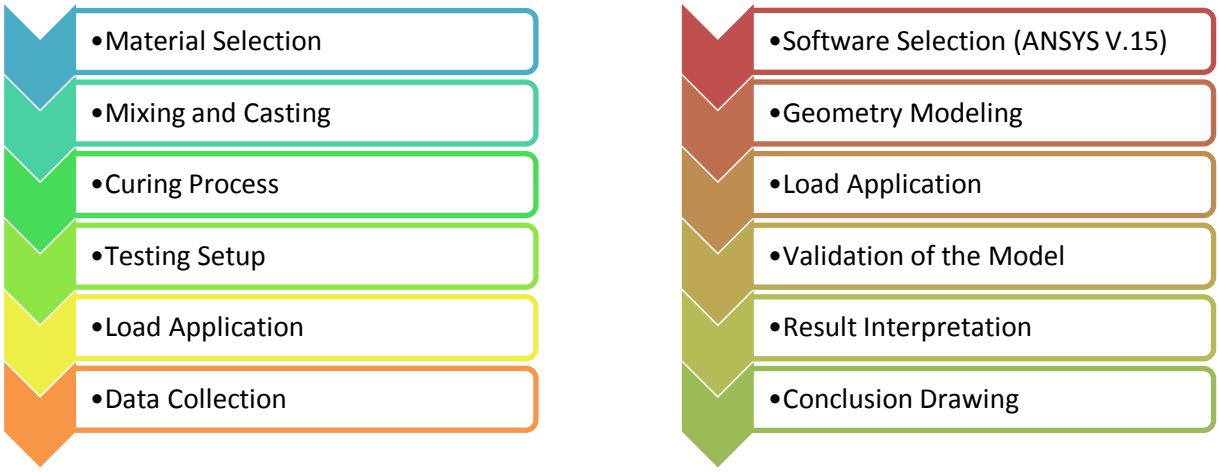

(a) Experimental approach (b) Numerical approach

Fig. 1. Flow chart of experimental and numerical methods.

3. Material Properties

The concrete mix included ordinary Portland cement CEMI 42.5N from the Suez factory, meeting the standards of E.S.S. 4756-1 (2013). For chemical and physical characteristics; the fine aggregate used was siliceous sand with a specific gravity of 2.6 kg/m^3, meeting E.S.S. 1109 (2008) standards. However, the coarse aggregate wasn't part of the mortar mix. To enhance strength and permeability, silica fume (S.F.) and fly ash partially replaced the cement by weight, while Polypropylene mesh e 300 was employed to enhance concrete properties. Pure, pollutant-free drinking water was utilized to mix and cure the ferrocement beams, with the addition of a superplasticizer to improve workability and facilitate the casting process CMB company provided it. It satisfies the super plasticizer criteria of ASTM-C-494 (2002). The reinforcement comprised steel bars measuring 8 mm and 10 mm in diameter, possessing respective yield strengths of almost 240 MPa and 360 MPa, meeting E.S.S. 1109 (2011) standards. Various types of reinforcing steel mesh, depicted in Fig. 2 were employed in the study. The technical specifications and mechanical properties of the expanded and welded steel mesh are detailed in Table 1 according to the producing companies and according to Shaheen et al. (2021).

Table 1. Properties of expanded and welded steel mesh as provided by the manufacturer.

Expanded steel mesh		Welded steel mesh	
Style	1532	Style	----
Sheet size	1 m × 10	Sheet size	1 m × 20
Weight	1.1 kg/m^2	Weight	0.44 kg /m^2
Diamond size	16 × 31 mm	Dimensions	12.5mm × 12.5 mm
Dimensions of strand	1.25 × 1.5 mm	Section diameter	0.7 mm
Proof stress	199 N/mm^2	Proof stress	400 N/mm^2
Proof strain	9.7×10^{-3}	Proof strain	1.17×10^{-3}
Ultimate strength	320 N/mm^2	Ultimate strength	600 N/mm^2
Ultimate strain	59.2×10^{-3}	Ultimate strain	58.8×10^{-3}

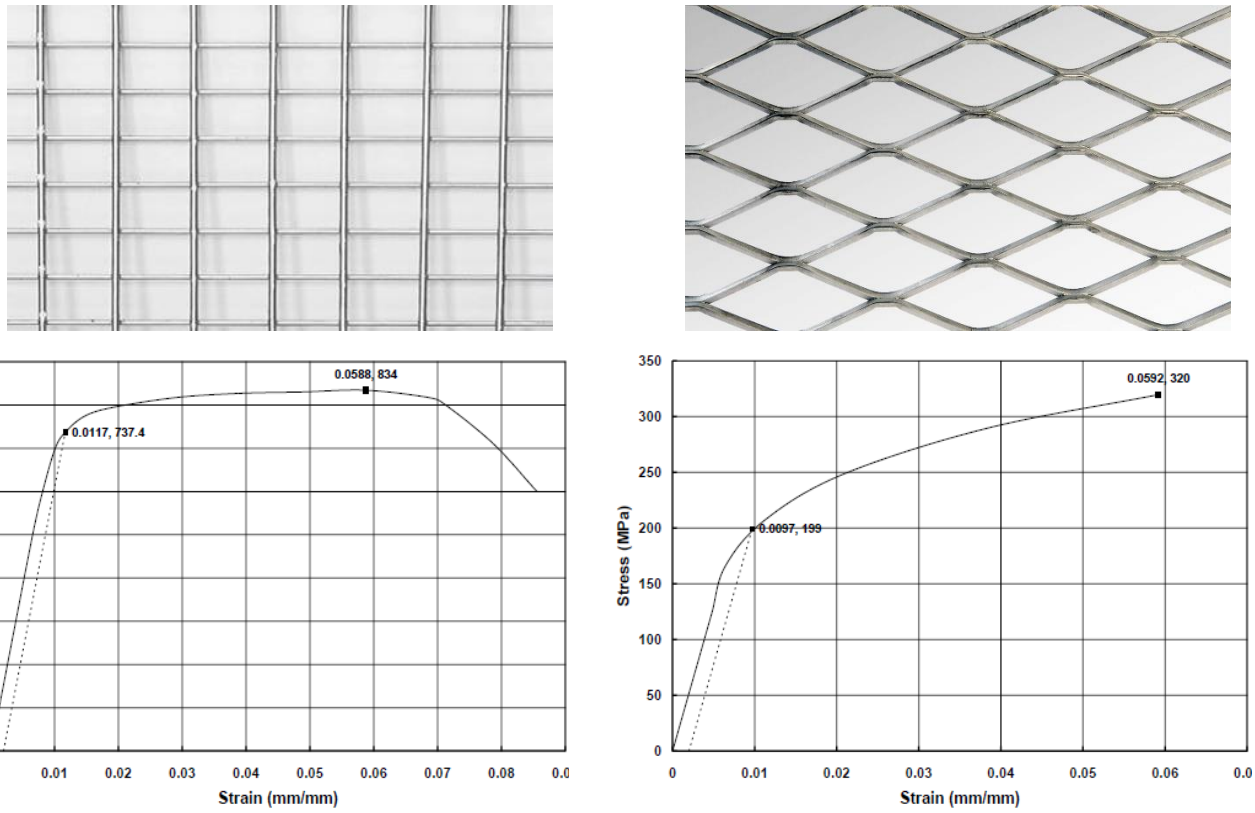

(a) Welded metal mesh (b) Expanded metal mesh

Fig. 2. Types of the steel metal meshes and their stress-strain relationship.

4. Experimental Work

In the construction material laboratory of Menoufia University in Egypt, fifteen beams were subjected to flexural loading analysis. These specimens were categorized into three sets based on their beam type refer to Table 2 and shown in Fig. 3. Group A contains standard rectangular reinforced concrete beam with the conventional reinforcement, whereas Group B utilized welded steel mesh surrounds the upper and lower steel bars for reinforcement, and Group C employed expanded steel mesh instead of welded steel mesh.

The beam dimensions are 1600 mm in length, 125 mm in width, and 200 mm in height, with openings strategically placed in the predicted critical shear and moment zones. The opening size was 50 mm in diameter which balanced to ensure functionality without compromising beam efficiency, allowing cable passage. Beams were tested under four-point loading until failure at a 1400 mm span. Fig. 3 depicts mesh preparation and casting.

The study focused on examining two main variables: the type of mesh used and the quantity and best location of openings. Throughout testing, vertical displacement concerning the load was meticulously recorded. The testing facility included control stations, loading cells, and a testing frame, with load increments ranging from 5.0 to 20 kN applied to all specimens. Deformation traits and crack patterns were thoroughly assessed at every loading stage in the experimental program conducted at Menoufia University's Faculty of Engineering laboratory in Egypt, dedicated to testing building materials.

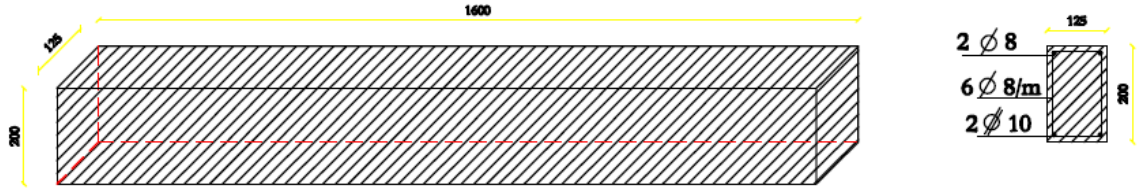

B con. standard rectangular reinforced concrete beam

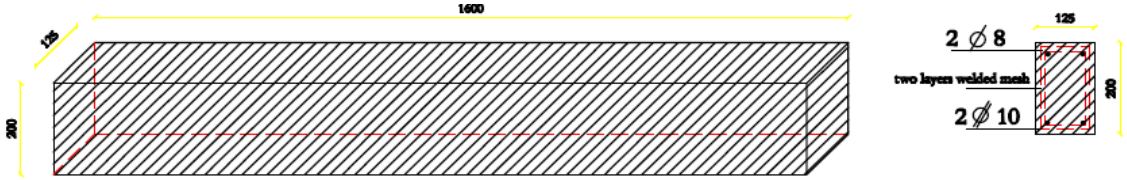

W 0 control welded mesh beam with no openings

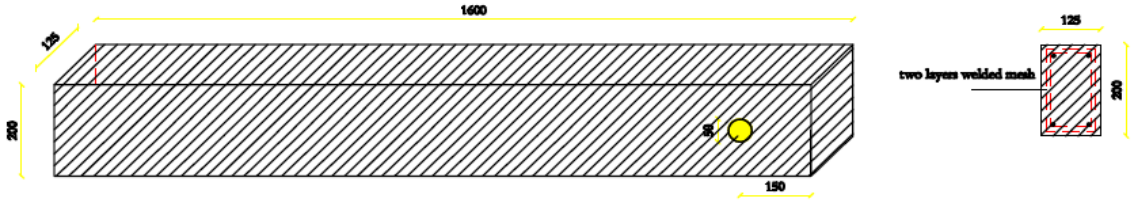

W_{H1} welded beam with one edge opening in horizontal direction

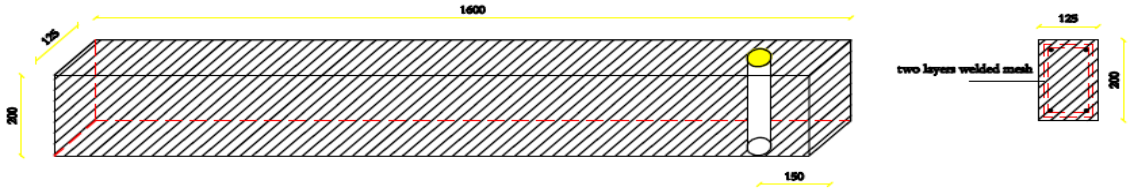

W_{V1} welded beam with one edge opening in vertical direction

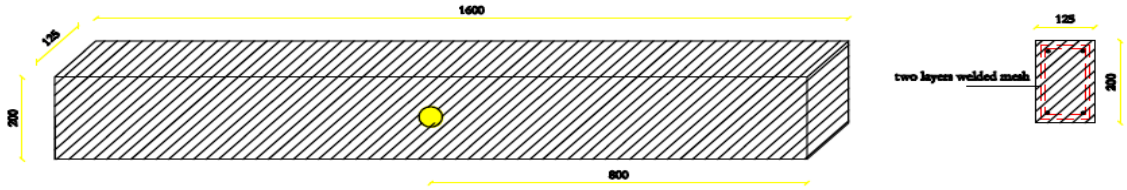

W_{H2} welded beam with one mid opening in horizontal direction

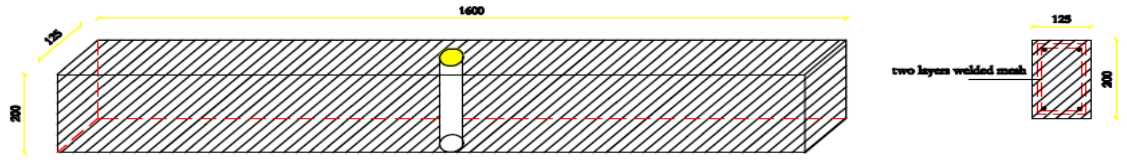

W_{V2} welded beam with one mid opening in vertical direction

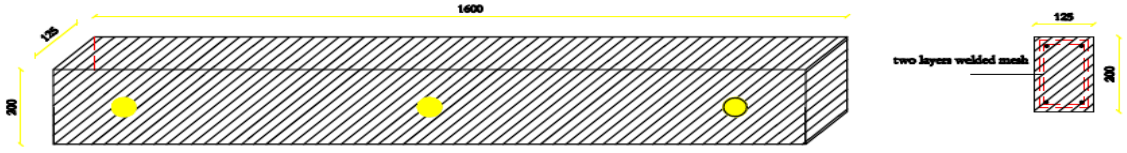

W_{H3} welded beam with three openings in horizontal direction

Fig. 3. (continued)

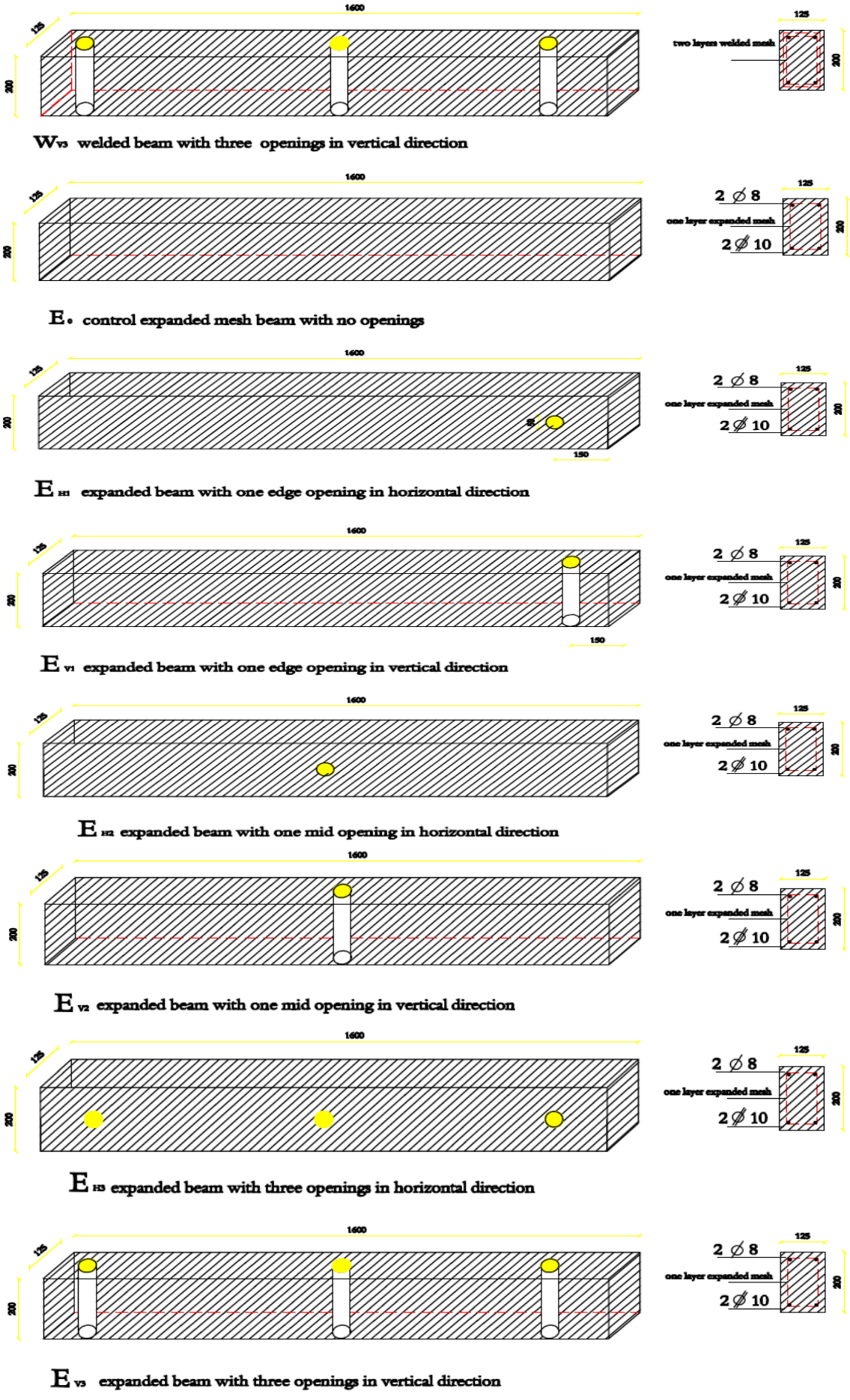

Fig. 3. Details of the tested beams.

Table 2. Details of the tested beams.

Groups	Beam no.	Designation of beams	Steel mesh			Reinforcing steel bars			Opening site and direction
			Type	No. of layers	Volume fraction (%)	Tensile	Compression	Stirrups	
A (R.C.)	1	B1	--	--	1.719	2Ø10	2Ø8	6Ø8 mm/m	--
B (welded)	2	W0	Welded wire mesh	2	1.379	2Ø10	2Ø8	--	--
	3	WH1		2	1.382	2Ø10	2Ø8	--	1 Hor. Edge
	4	WV1		2	1.392	2Ø10	2Ø8	--	1 Ver. Edge
	5	WH2		2	1.382	2Ø10	2Ø8	--	1 Hor. Mid
	6	WV2		2	1.392	2Ø10	2Ø8	--	1 Ver. Mid
	7	WH3		2	1.382	2Ø10	2Ø8	--	3 Hor.
	8	WV3		2	1.418	2Ø10	2Ø8	--	3 Ver.
C (expanded)	9	E0	Expanded steel mesh	1	1.577	2Ø10	2Ø8	--	--
	10	EH1		1	1.586	2Ø10	2Ø10	--	1 Hor. Edge
	11	EV1		1	1.592	2Ø10	2Ø8	--	1 Ver. Edge
	12	EH2		1	1.586	2Ø10	2Ø8	--`	1 Hor. Mid
	13	EV2		1	1.592	2Ø10	2Ø8	--	1 Ver. Mid
	14	EH3		1	1.606	2Ø10	2Ø8	--	3 Hor.
	15	EV3		1	1.624	2Ø10	2Ø8	--	3 Ver.

4.1. Specimen preparation and test setup

4.1.1. Mortar matrix

A mortar matrix, prioritizing high flowability, strength, and compaction, composed of ordinary Portland cement (type I), potable water, and fine sand, with a low water-cement ratio of 0.35, was used in the specimens to influence the behavior of the ferrocement units by ensuring effective permeation through the layers of steel mesh reinforcement. To enhance flow characteristics and expedite early strength development, a super plasticizing agent was employed. Super plasticizer was used in the mix 2 % of the cement weight, to provide the mortar mix with high workability to ensure ease the process of casting. The sand/cement ratio was 2.0, with a 10% replacement of cement by fly ash, and the addition of fiber e300 at a rate of 0.9 kg/m3, equal to 0.2% of the cement weight. After 28 days, the average compressive strength of the ferrocement mortar reached 25 MPa. A mechanical mixer used in the laboratory for all mixes, with constituent materials initially dry mixed, followed by the addition of blended water and further mixing. Mechanical compaction was applied to all beams in the experiment. All materials used were tested according to Egyptian standard specifications (E.S.S.) to determine their physical and mechanical properties. Additionally, visual inspections were conducted to ensure cleanliness and apparent quality.

4.1.2. Casting and curing

Rectangular molds, constructed from contrasting wood as shown in Fig. 4, were used for beam formation. The precise locations for the required openings in each beam are carefully determined, followed by cutting the corresponding sections of the metal mesh to create these openings. To preserve the integrity of the shape and structure during casting, these openings are filled with foam or a hollow plastic pipe with the same required diameter, which is carefully removed before the final setting of the concrete, ensuring accurate and consistent results in the final beam. After placing foam in the openings, a mesh frame was added to the molds, and the concrete casting and mixing were done uniformly for all mixes. The dry mix of sand and cement was gradually combined with water and admixture to achieve a uniform mixture in about ten minutes. The beams were then left in the molds for a full day in laboratory conditions until the burlap-covered sides formed.

4.1.3. Test set-up and instrumentation

Following a 28-day period, white paint was used on the beams to aid in crack detection during testing. For strain measurement against load, four demec points were positioned on both the upper and lower sides at the mid-span of one side of the beam, as depicted in Fig. 5.

All specimens were tested using a loading frame, employing a four-point loading technique with a consistent 1400 mm distance between supports, centering the specimen on the test apparatus; loads, spaced 73 cm from the beam's ends, were applied. Two dial gauges were fixed to upper and lower demec points, and a hydraulic jack, with a maximum capacity of 80.0 kN, increased the load incrementally by 5 kN to 20 kN.

Strain values were calculated by multiplying readings with the gauge factor of the mechanical gauge used, and beam deflection was assessed by recording dial gauge readings at each load increment, as depicted in Fig. 6. Cracks along the specimen's side were traced and marked, noting the initial crack load, crack propagation, and failure mode for each specimen, with the load continually increased until fracture occurred.

Fig. 4. Phases of specimen preparation until the casting and curing process.

Fig. 5. Positions of the demec points on the loaded beams.

Fig. 6. The dial gauge and deflection gauge used in the study.

5. Results and Discussion

The results, including first cracking load, ultimate load, ductility ratio, and energy absorption, are presented in Table 3, with measurements obtained during the test encompassing cracking load, ultimate load, deflection at the first cracking load, and deflection at the ultimate load, while ductility ratio and energy absorption were calculated from the load versus deflection diagram for each tested beam.

Table 3. Experimental outcomes of the structural behavior of the tested beams.

Groups	Beam no.	Vr (%)	First crack load (kN)	Deflection at first load crack (mm)	Ultimate load (kN)	Deflection at ultimate load (mm)	Ductility ratio	Energy absorption (kN·mm)
A (control)	Bcon	1.719	5.0	0.41	58.8	18.02	43.95	776.4
B (welded)	W0	1.379	5.0	0.39	56.7	8.23	21.10	364.9
	WH1	1.382	10.0	1.13	41.2	6.87	6.08	258.9
	WV1	1.392	5.0	0.70	44.9	5.15	7.36	128.8
	WH2	1.382	8.0	1.02	27.7	6.12	6.00	151.9
	WV2	1.392	11.0	0.92	55.7	8.17	8.88	417.3
	WH3	1.382	5.0	0.44	38.9	5.80	13.18	256.7
	WV3	1.418	14.0	1.30	59.8	7.21	5.55	307.7
C (expanded)	E0	1.577	5.0	0.16	67.3	19.63	54.53	1027.3
	EH1	1.586	11.0	0.78	42.6	4.96	6.36	177.8
	EV1	1.592	11.0	0.83	57.2	6.15	7.41	281.2
	EH2	1.586	14.0	1.22	50.3	6.03	4.94	263.8
	EV2	1.592	11.0	1.07	57.6	6.89	6.44	313.6
	EH3	1.606	11.0	0.74	51.4	5.11	6.91	248.5
	EV3	1.624	8.0	0.47	46.5	9.40	20.00	3364.0

5.1. First crack loads and ultimate loads

The first crack appeared as a vertical flexural crack in the lower part of the mid-span. Fig. 7 shows the first cracking and ultimate load values for all tested beams. Beam E0 recorded the highest ultimate load at 67.3 kN, while beam WH2 had the lowest at 27.7 kN. Beams Wv3 and EH2 had the highest first cracking load at 14.0 kN, whereas beams B con, W0, WH1, WV1, WH3, and E0 had the lowest first cracking load at 5.0 kN. Beams reinforced with expanded steel meshes demonstrated higher ultimate loads than those with welded steel meshes, with increases of 3.39%, 81.59%, and 32.13% for beams with one edge, one mid, and three horizontal openings, respectively. For vertical openings, expanded steel mesh beams showed a 27.39% higher ultimate load in edge openings and a 3.41% increase in mid-openings compared to welded steel meshes. However, for beams with three vertical openings, the ultimate load decreased by 22.2% with expanded steel meshes compared to welded meshes. Overall, beams with openings had an average ultimate load reduction of 26.85% for welded steel mesh and 32.13% for expanded metal mesh beams compared to beams without openings.

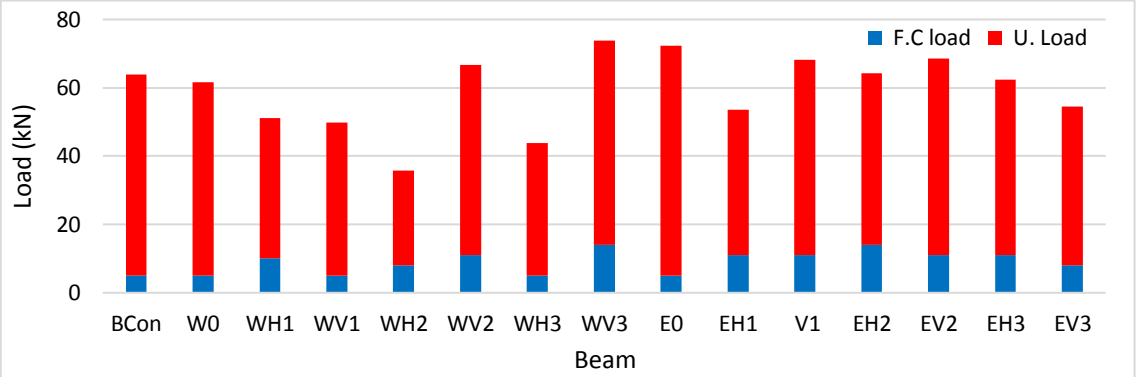

Fig. 7. First crack load and ultimate load values of the tested beams.

5.2. Ductility ratio

The ductility ratio, which is a measure of a beam's ability to undergo deformation before failure, is determined by comparing the mid-span deflection at the ultimate load (Δu) to the deflection at the first cracking load (Δy). This ratio ($\Delta u/\Delta y$) was found to be higher in beams that were reinforced with expanded mesh as opposed to those reinforced with welded mesh. This indicates that beams with expanded mesh reinforcement can endure greater deformation before failing, making them more ductile. The specific ductility ratio values for each tested beam are provided in Table 3 and illustrated in Fig. 8.

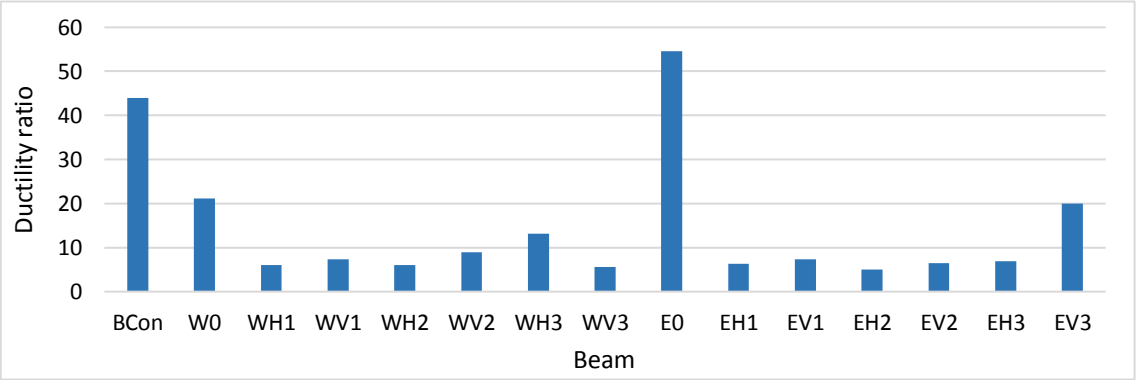

Fig. 8. Ductility ratio values of the tested beams.

5.3. Energy absorption

Energy absorption refers to the total amount of energy a beam can absorb before failure, which is represented by the area under the load-deflection curve. To determine this value for each beam specimen, the load-deflection curve equation was integrated. The resulting energy absorption values for all the tested beams are listed in Table 3. Additionally, Fig. 9 visually compares these values, showing that beams reinforced with expanded mesh absorbed more energy than those reinforced with welded mesh. This suggests that expanded mesh reinforcement enhances the beam's capacity to absorb energy before failing.

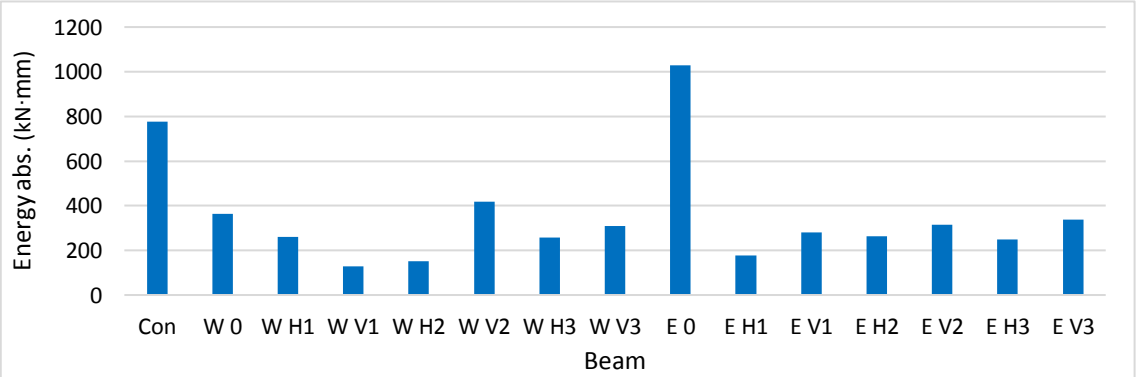

Fig. 9. Energy absorption values for the tested beams.

5.4. Load versus deflection relationship

According to Table 4, the relationship between applied load and deflection in tested beams can be analyzed by considering the orientation of the mesh openings and the type of mesh used (welded or expanded steel mesh). These factors influence the load-deflection behavior and overall structural performance of the beams.

Figs. 10 and 11 shows how the orientation of the openings impacts the load-deflection curve, while Figs. 12–14 demonstrates the effect of the mesh type.

Table 4. First crack and ultimate loads and their equivalent deflection for all tested beams.

Beam no.	Bcon	W0	WH1	WV1	WH2	WV2	WH3	WV3	E0	EH1	EV1	EH2	EV2	EH3	EV3
First crack load (kN)	5.00	5.00	10.00	5.00	8.00	11.00	5.00	14.00	5.00	11.00	11.00	14.00	11.00	11.00	8.00
Deflection at F.C.L. (mm)	0.41	0.39	1.13	0.70	1.02	0.92	0.44	1.30	0.16	0.78	0.83	1.22	1.07	0.74	0.47
Ultimate load (kN)	58.80	56.70	41.20	44.90	27.70	55.70	38.90	59.80	67.30	42.60	57.20	50.30	57.60	51.40	46.50
Deflection at U.L. (mm)	18.02	8.23	6.86	5.15	6.12	8.17	5.80	7.21	19.63	4.96	6.15	6.03	6.89	5.11	9.40

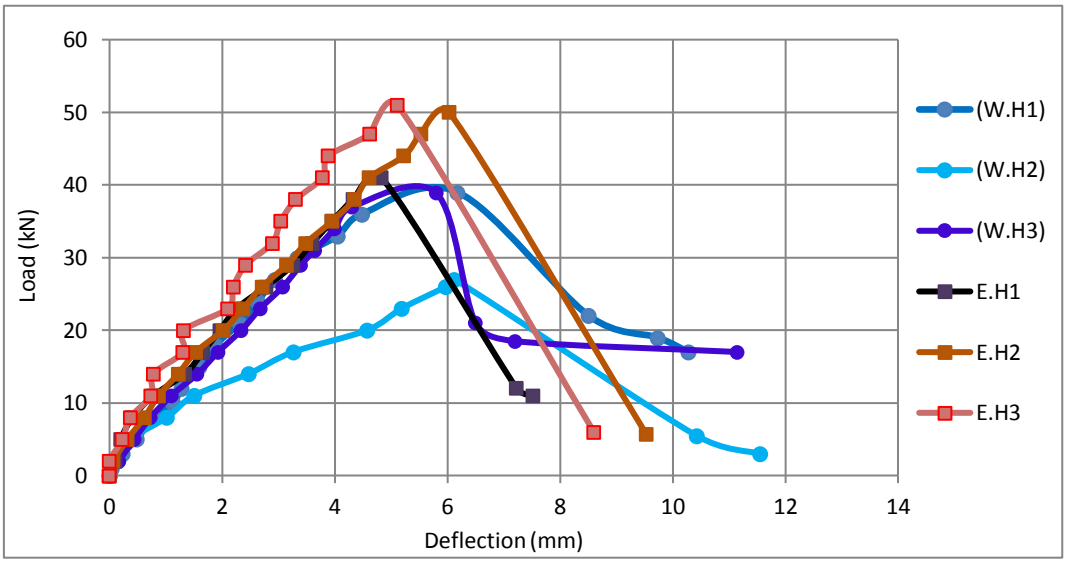

Fig. 10. Load vs. deflection for the beams with horizontal openings.

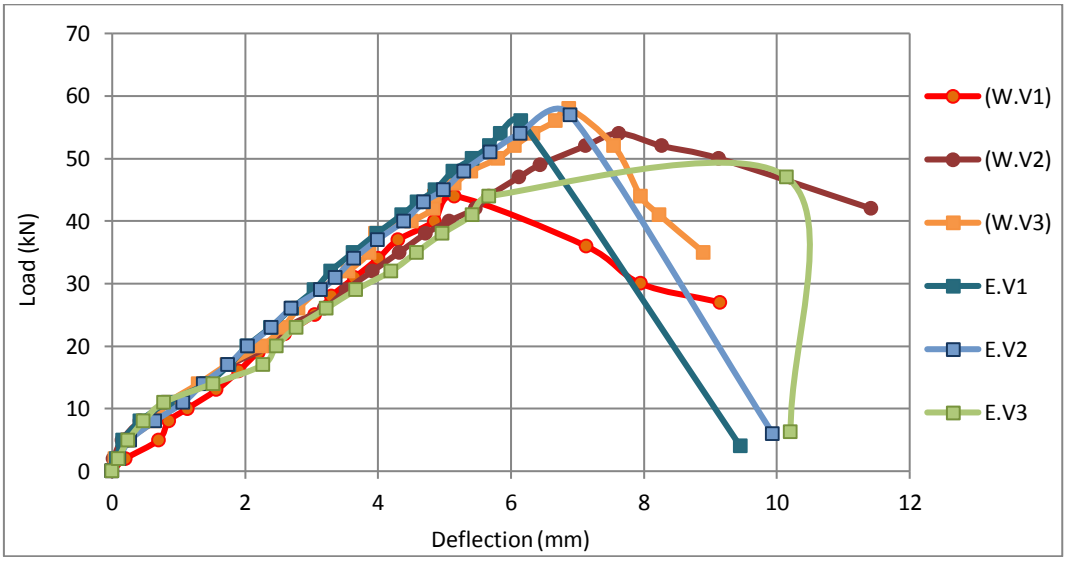

Fig. 11. Load vs. deflection for the beams with vertical openings.

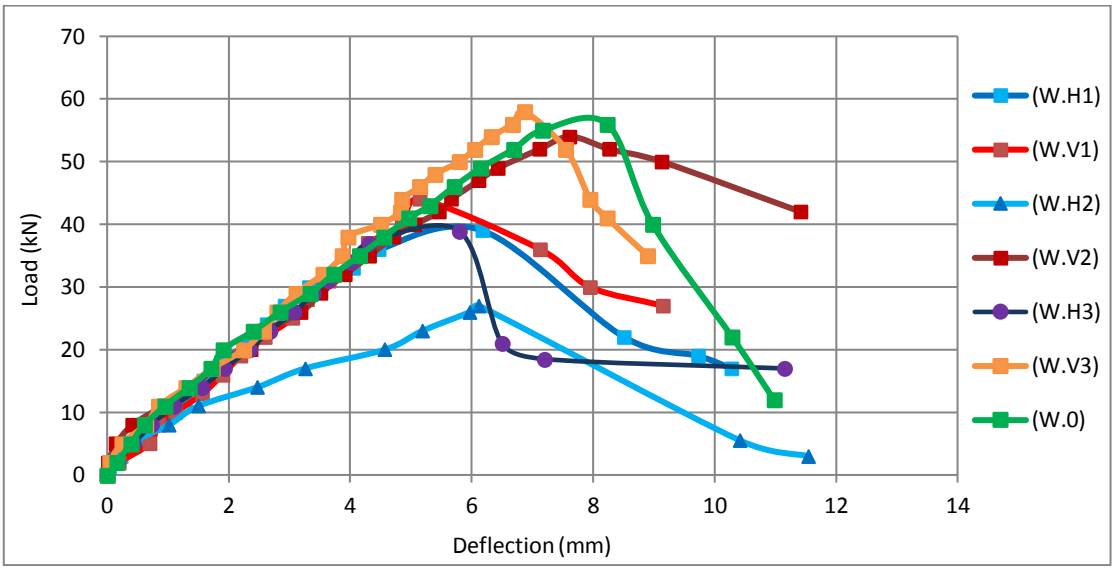

Fig. 12. Load vs. deflection for welded metal mesh beams Group (B).

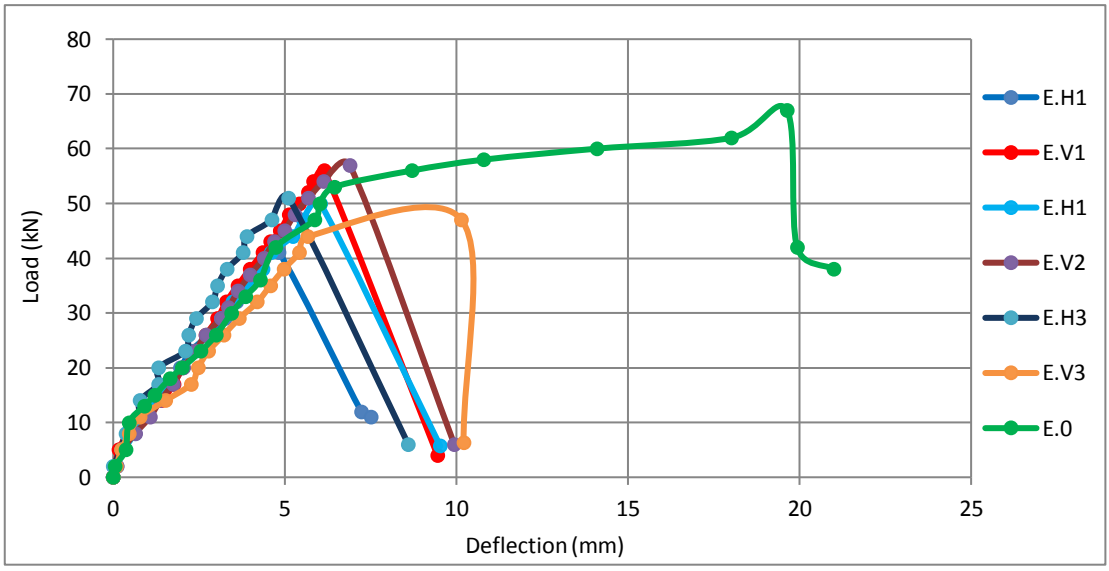

Fig. 13. Load vs. deflection for expanded metal mesh beams Group (C).

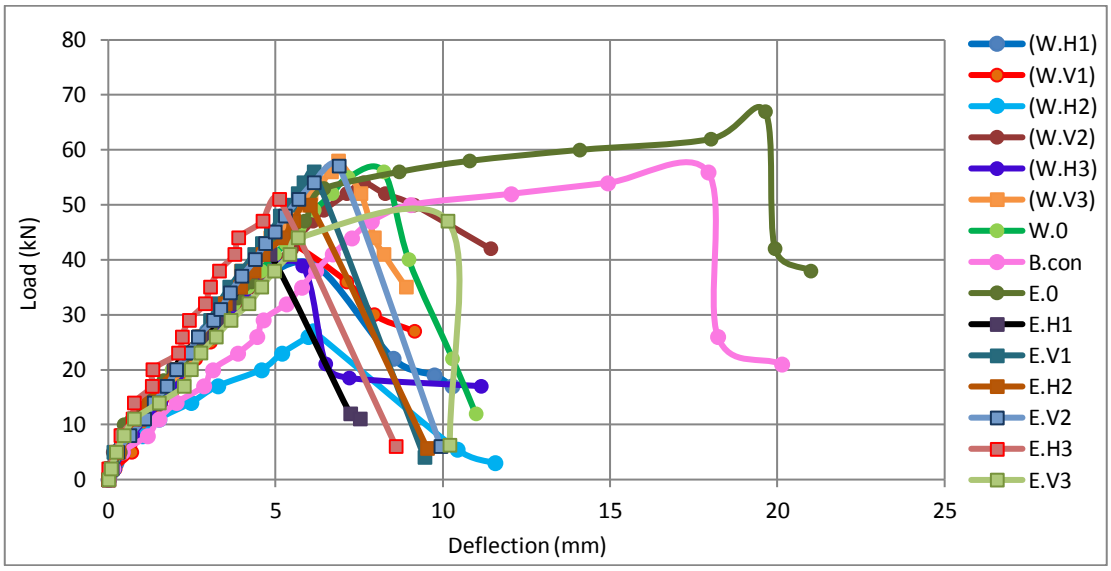

Fig. 14. Load vs. deflection for the tested beams.

For Group (B), the load-deflection relationship was almost linear up to roughly 56.7 kN, 41.2 kN, 44.9 kN, 27.7 kN, 55.7 kN, 38.9 kN, and 59.8 kN for beams W0, WH1, WV1, WH2, WV2, WH3 and WV3, respectively, when the deviations from the linear relationship began. The maximum deflection for beams W0, WH1, WV1, WH2, WV2, WH3 and WV3, was 8.26mm, 6.48 mm,5.37 mm, 6.26 mm, 8.17 mm, 5.80 mm and 7.07 mm, respectively, as shown in Fig. 12.

For Group (C), the load-deflection relationship was almost linear up to roughly 67.3 kN, 42.6 kN, 57.2 kN, 50.3 kN, 57.6 kN, 51.4 kN, and 46.5 kN for beams E0, EH1, EV1, EH2, EV2, EH3 and EV3, respectively, when the deviations from the linear relationship began. The maximum deflection for beams E0, EH1, EV1, EH2, EV2, EH3 and EV3, respectively, was 19.633 mm, 4.96 mm,6.23 mm, 6.05 mm, 6.93 mm, 5.14 mm and 9.4 mm, respectively, as shown in Fig. 13.

Beams with vertical mesh openings (e.g., WV1, WV2, WV3, EV1, EV2, EV3) generally exhibit higher first crack loads compared to those with horizontal openings (e.g., WH1, WH2, WH3, EH1, EH2, EH3). This suggests that vertical openings provide better resistance to initial cracking. The deflection values at the first crack load vary significantly, with beams reinforced with expanded mesh (e.g., E0, EH1, EV1) generally showing higher deflections compared to those with welded mesh. This indicates that expanded mesh allows for more flexibility before the first crack occurs. The ultimate load capacity varies, with some beams (e.g., E0, WV3) achieving high ultimate loads, indicating superior strength. However, beams with horizontal mesh openings (e.g., WH1, WH2) tend to have lower ultimate load values, suggesting that horizontal orientations may be less effective in enhancing the beam's load-bearing capacity. The deflection at ultimate load shows a wide range, with some beams (e.g., Bcon, E0) exhibiting large deflections, indicating high ductility. Beams with vertical openings (e.g., WV3, EV2) generally demonstrate moderate deflections, balancing strength and flexibility. This analysis highlights how the orientation of mesh openings and the type of mesh reinforcement influence both the strength and ductility of the beams, with vertical openings and expanded mesh generally offering better performance.

We also notice for beams reinforced with expanded steel mesh, it is evident that the control beam (E0) experienced failure due to bending, resulting in higher bending moments and, consequently, greater deflection values. In contrast, beams EH1, EV1, EH2, EV2, EH3, and EV3 exhibited lower deflection values even at reduced loads. This reduction in deflection is attributed to the redistribution of stresses, with some stresses being redirected around the openings in the shear zone while the remaining stresses were absorbed by the bending zone. This stress distribution effectively minimized deflection in these beams. The ultimate load for beams E0, EH1, EV1, EH2, EV2 and EH3 increased by 18.7%, 3.39%, 27.4%, 81.59%, 3.41% and 32.13 percent, respectively, in comparison to beams W0, WH1, WV1, WH2, WV2 and WH3 while EV3 was less than WV3 by 22.24 percent.

5.5. Compressive and tensile strains

According to Table 5, all of the tested beams' loads versus strain curves are shown in Figs. 15 and 16. The load-strain relationship was nearly linear until the first cracking load, at which point it started to deviate from the linear relationship.

Table 5. Compressive and tensile strains at first crack load and ultimate load for all tested beams.

Beam no.	Bcon	W0	WH1	WV1	WH2	WV2	WH3	WV3	E0	EH1	EV1	EH2	EV2	EH3	EV3
First crack load (kN)	5.00	5.00	10.00	5.00	8.00	11.00	5.00	14.00	5.00	11.00	11.00	14.00	11.00	11.00	8.00
Compressive strain at F.C.L. (mm)	-0.016	-0.043	-0.049	-0.002	-0.063	-0.082	-0.023	-0.123	-0.021	-0.062	-0.029	-0.024	-0.089	-0.054	-0.025
Tensile strain at F.C.L. (mm)	0.047	0.012	0.072	0.047	0.0445	0.0541	0.0443	0.0945	0.004	0.090	0.188	0.136	0.089	0.0436	0.033
Ultimate load (kN)	58.80	56.70	41.20	44.90	27.70	55.70	38.90	59.80	67.30	42.60	57.20	50.30	57.60	51.40	46.50
Compressive strain at F.C.L. (mm)	-0.290	-0.269	-0.145	-0.073	-0.131	-0.397	-0.181	-0.348	-0.46	-0.144	-0.124	-0.142	-0.316	-0.178	-0.22
Ultimate load (kN)	2.082	0.415	0.288	0.284	0.170	0.484	0.903	0.474	2.372	0.293	0.824	0.474	0.508	0.391	1.651

For Group (B), the compressive strain increased with the increase of the applied load as shown in Fig. 5. For beams W0, WH1, WV1, WH2, WV2, WH3 and WV3 the maximum compressive strain reached approximately -0.2694, -0.14534, -0.0739, -0.13153, -0.3973, -0.1810, and -0.3488 respectively at maximum load 56.7 KN, 41.2 KN, 44.9 KN, 27.7 KN, 55.7 KN, 38.9 KN, and 59.8 KN. However, the maximum tensile strain for W0, WH1, WV1, WH2, WV2, WH3 and WV3 was approximately 0.41542, 0.2886, 0.2847, 0.1703, 0.4843, 0.9035, and 0.4749 respectively at a maximum load.

The load-strain curve behavior can be delineated into three main zones: the uncracked zone, where strain values are nearly zero from zero loads to the first crack load; the cracking zone, characterized by a linear relationship between loads and strain, resulting in increased strain values due to crack formation; and the crack propagation zone, consisting of two sub-zones, the first with

lower strain values due to mesh resistance to stresses and the second displaying the highest strain values as loads increase with cracks propagation. For Group (C), the compressive strain increased with the increase of the applied load as shown in Fig. 16. For beams E0, EH1, EV1, EH2, EV2, EH3 and EV3 the maximum compressive strain reached about -0.4616, -0.14419, -0.1247, -0.14204, -0.3169, -0.1783 and -0.2262 respectively at maximum load 67.3 KN, 42.6 KN, 57.2 KN,50.3 KN, 57.6 KN, 51.4 KN, and 46.5 KN. However, as shown in Fig. (13.b) the max tensile strain for beams E0, EH1, EV1, EH2, EV2, EH3 and EV3 was 2.3728, 0.29302, 0.82461, 0.47403, 0.50857, 0.3910 and 1.65141 respectively at a maximum load.

A potential explanation lies in the observation that for beam E0, the initial cracks were primarily attributed to bending, resulting in a lower first crack load compared to beams EH1, EV1, EH2, EV2, EH3, and EV3. In these latter beams, the cracks were a combination of both bending and shear cracks, particularly in shear zones, as the number of openings increased. This combination led to concentrated stresses around the openings in shear zones, ultimately enhancing the first crack load due to the heightened shear strength of the expanded mesh.

5.6. Impact of openings on the beam performance

In beams with three openings in a horizontal direction, the ultimate load for welded steel mesh beams was 31.4% lower than beams without openings, this indicates that horizontal openings significantly reduce the load-bearing capacity of welded steel mesh beams, while for expanded mesh beams, it was 23.6% lower. Conversely, in beams with three openings in a vertical trend, the ultimate load for welded steel mesh beams was 5.46% greater than beams without openings, this suggests that vertical openings may enhance the load-bearing capacity of welded mesh beams. However, for expanded mesh beams, it was 30.9% lower indicating that vertical openings significantly weaken expanded mesh beams. The maximum deflection of welded beams with three openings in a horizontal trend decreased by 29.5%. This reduction suggests improved rigidity or reduced bending in these beams. For expanded beams, it decreased by 74% indicating a significant improvement in stiffness and reduced bending, compared to beams with no openings. In a vertical trend, the maximum deflection for welded beams decreased by 12.4% reflecting a moderate improvement in rigidity, while for expanded beams, it decreased by 108.8% which might be due to an increased capacity to absorb loads or a different failure mode, leading to less deflection. The ductility ratio of welded beams with three openings decreased by 55.6% suggesting that the ability of these beams to undergo deformation before failure is significantly reduced with horizontal openings. For expanded beams, it decreased by 63% indicating a substantial reduction in ductility similar to welded mesh beams, both compared to beams with no openings. This analysis is based on the findings presented in Table 3.

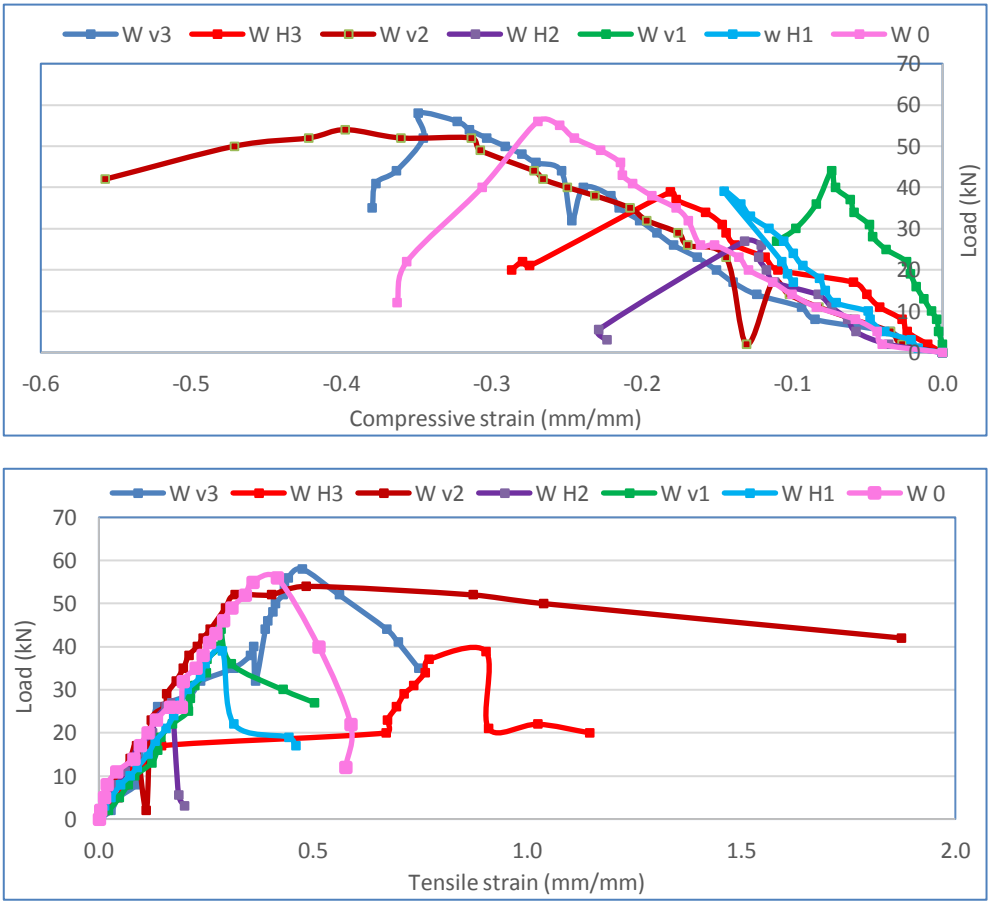

Fig. 15. Load vs. strain curves of welded mesh beams Group (B).

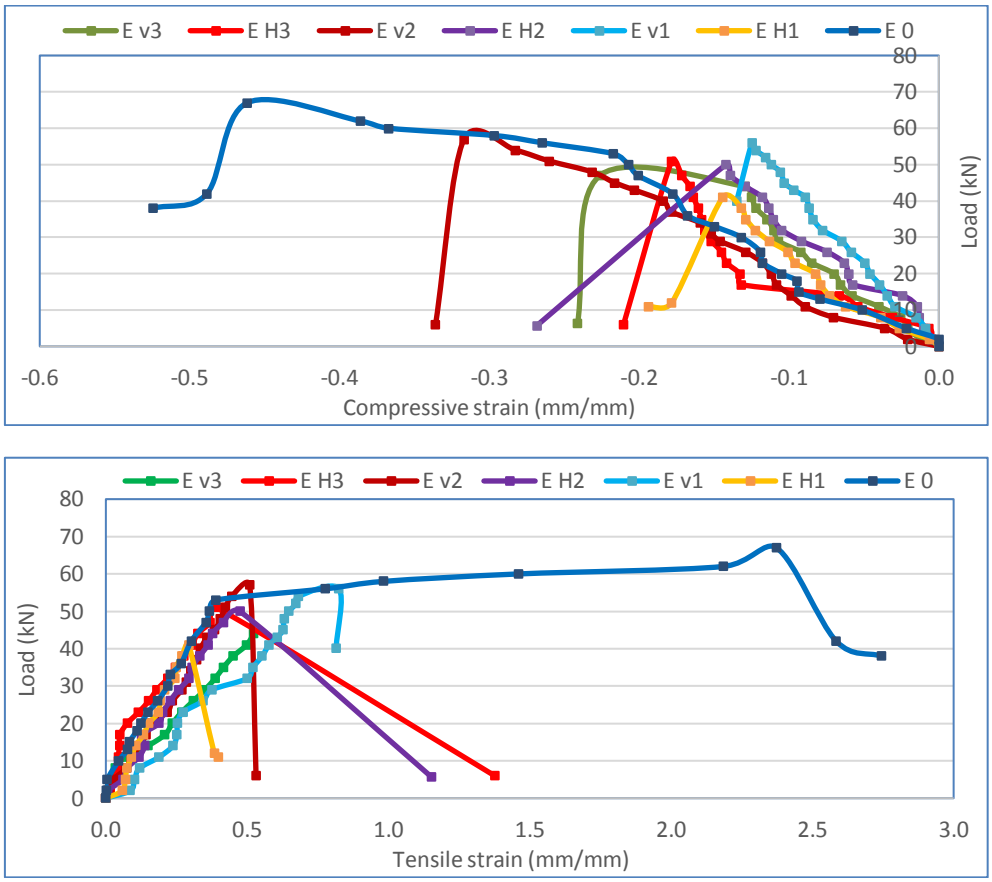

Fig. 16. Load vs. strain curves of expanded mesh beams Group (C).

5.7. Cracking patterns and failure modes

Cracks on the side of the beam were labeled and observed, documenting the first crack load, crack propagation, and failure mechanism for each beam. Initial flexural cracks appeared near the mid-span and shear cracks initially emerged near the left and right supports, developing diagonally across the shear span. With increasing load, cracks extended vertically and propagated more rapidly. As the load approached failure, the cracks widened, especially at mid-span, where some cracks almost reached the top surface of the beam. The presence of steel mesh played a role in regulating crack width. In Fig. 17, the cracks in all tested beams are depicted, highlighting a combination of shear and bending failure as the primary cause, with bending exerting the most significant influence. The cracking patterns and failure modes of beams with openings, reinforced with both welded and expanded metal meshes, exhibited a combination of shear and bending failures. However, shear was the predominant factor influencing the overall failure behavior.

6. Numerical Model Results

The finite element method is widely acknowledged as the most extensive, powerful, and mature technology in research and engineering applications. This study investigates the nonlinear shear behaviors of reinforced concrete beams with circular openings using the structural analysis program ANSYS V. 15.20. The parameters studied include the position and direction of the opening in both welded and expanded layer mesh. The load-deflection curve is crucial in studying the behavior of beams as it illustrates various response parameters such as ultimate load, deflection, and cracks.

6.1. Geometry, modeling, loads, and boundary conditions

For concrete modeling, an eight-node solid element (SOLID65) is utilized, with three translational and extra rotational degrees of freedom at each node, with a strength of 25 MPa, defined for both linear and nonlinear states. This element accounts for plasticity, cracking, large deflections, and plastic deformation. The beams were modeled using a mesh size of 50×50×50 mm. Steel bars and stirrups were represented using Link 180 elements, with yield stresses of 360 MPa for the main reinforcement steel bars and 280 MPa for the secondary reinforcement bars. Steel plates with dimension 125 x 50 mm were modeled using SOLID185 elements to simulate the loading and bearing plates, regarding the welded and expanded meshes, each installment was evaluated similarly to stirrups. The loading stage was handled as a displacement process. For the support conditions, at the two lines of contact with the roller supports underneath, the bottom surface of the beam was installed to be fixed to prevent translation in the XZ, XY, and YZ directions as well as rotation about the XY direction, as shown in Fig. 18. Tables 7 and 8 provide the properties of the concrete and steel.

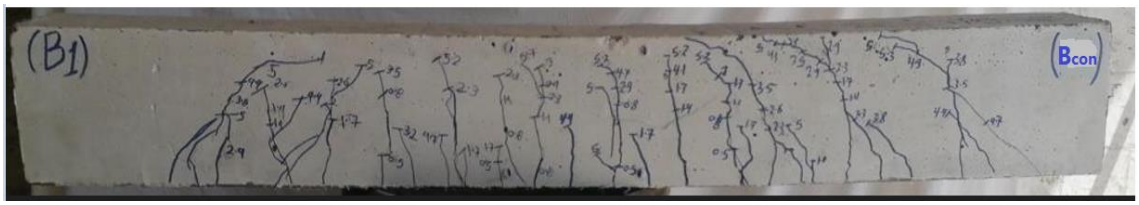

Cracking patterns for control beam (B0)

(a) Beam of the Group A (standard rectangular reinforced concrete beam)

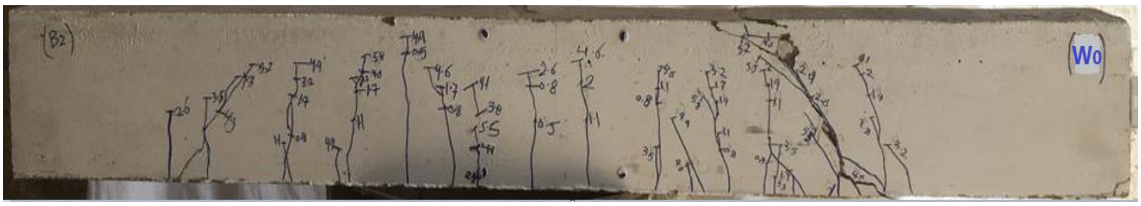

Cracking patterns for control welded beam (W0)

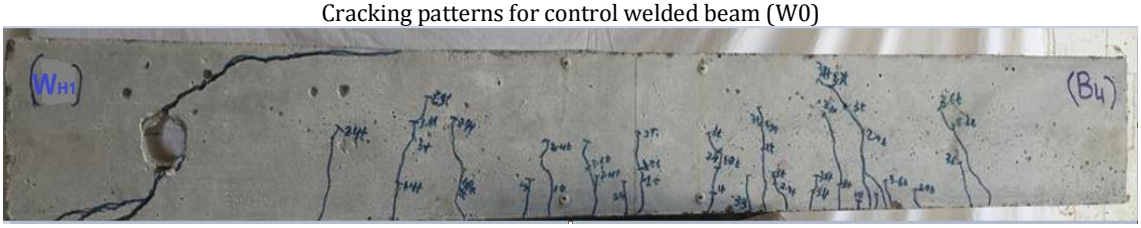

Cracking patterns for beam (WH1)

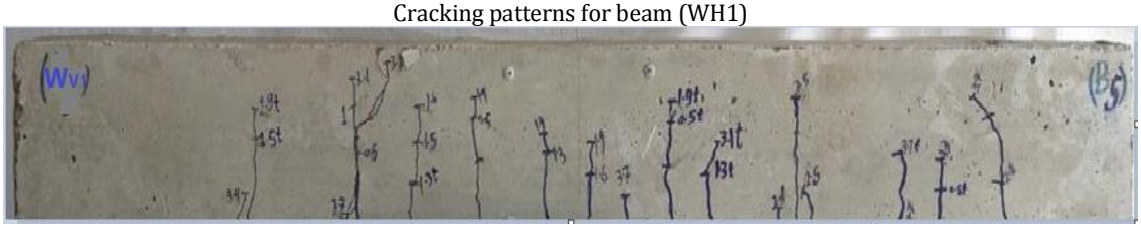

Cracking patterns for beam (WV1)

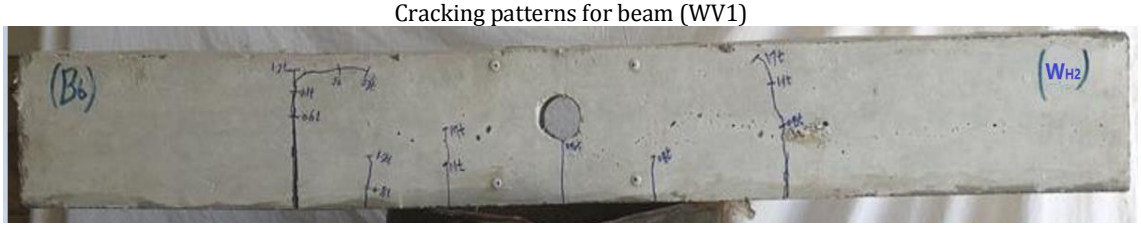

Cracking patterns for beam (WH2)

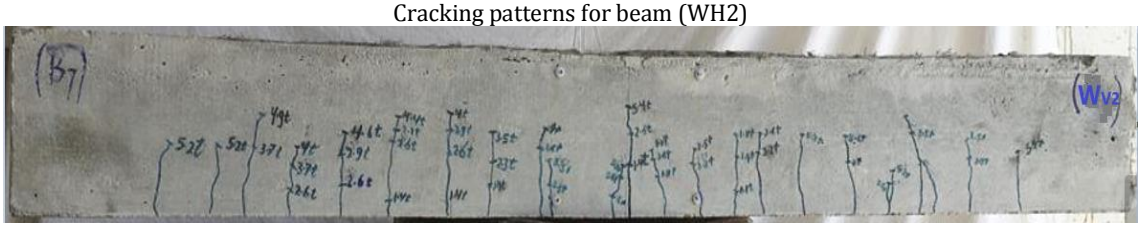

Cracking patterns for beam (WV2)

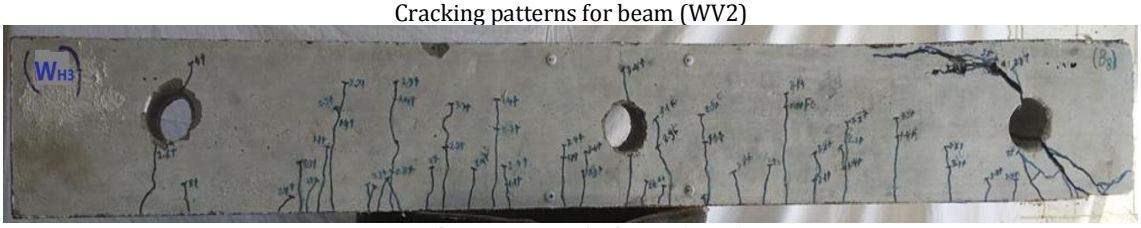

Cracking patterns for beam (WH3)

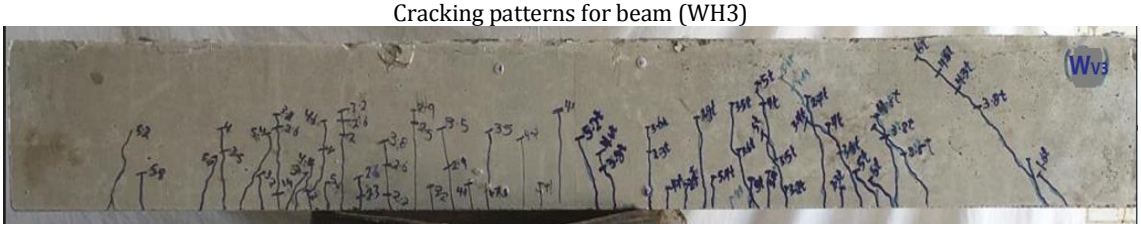

Cracking patterns for beam (Wv3)

(b) Beams of the Group B with welded mesh.

Fig. 17. (continued)

Cracking patterns for control expanded beam (E0)

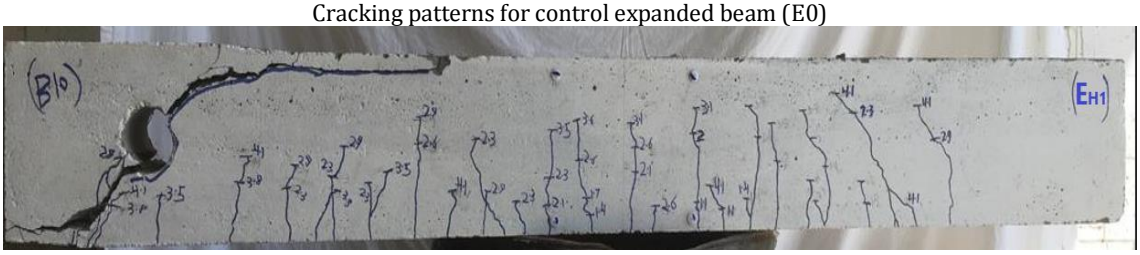

Cracking patterns for beam (EH1)

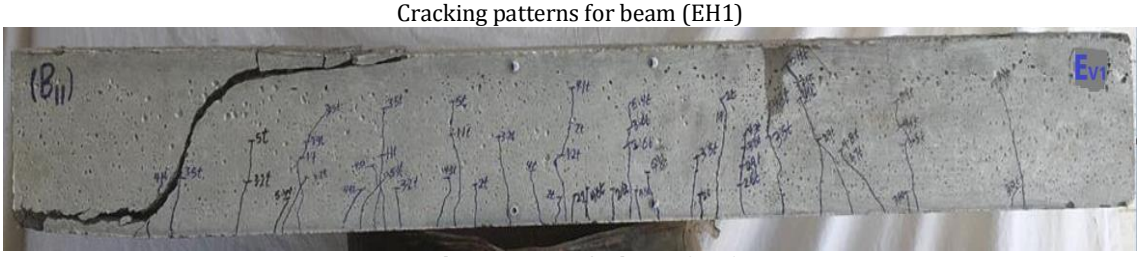

Cracking patterns for beam (EV1)

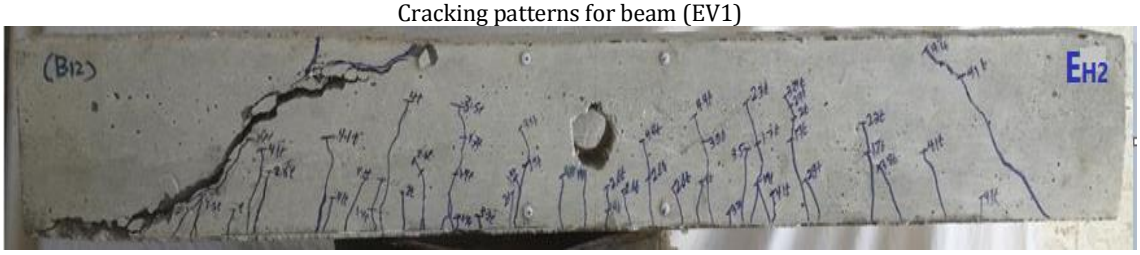

Cracking patterns for beam (EH2)

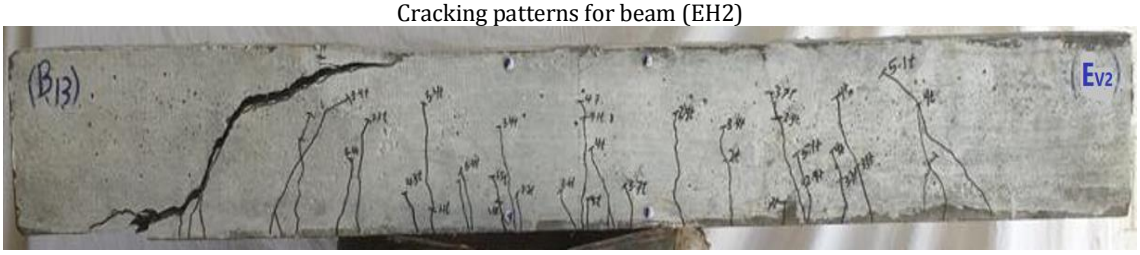

Cracking patterns for beam (EV2)

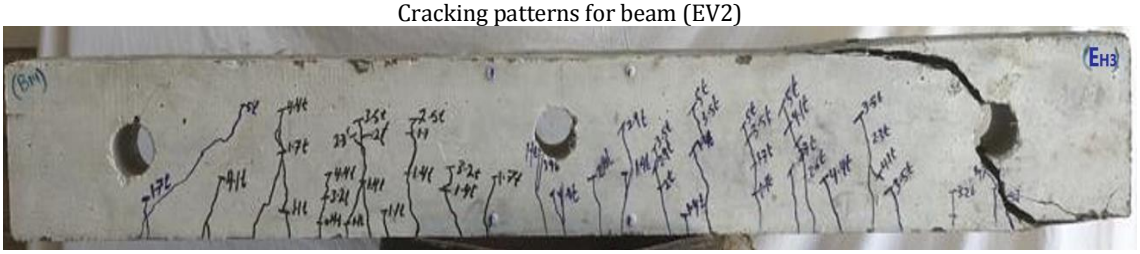

Cracking patterns for beam (EH3)

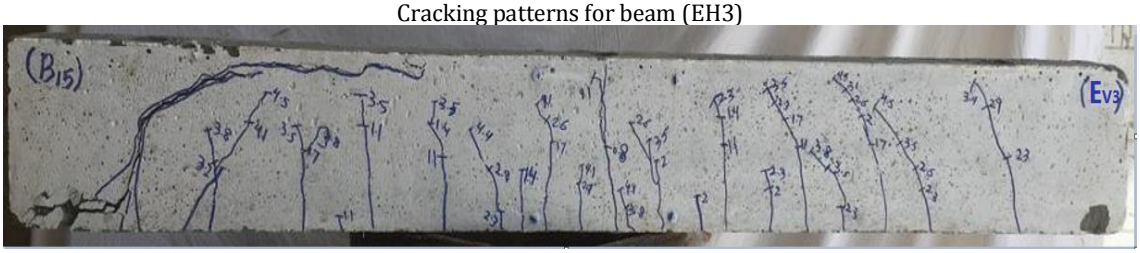

Cracking patterns for beam (EV2)
(c) Beams of the group C with expanded mesh.

Fig. 17. Cracking patterns and failure modes of the tested beams.

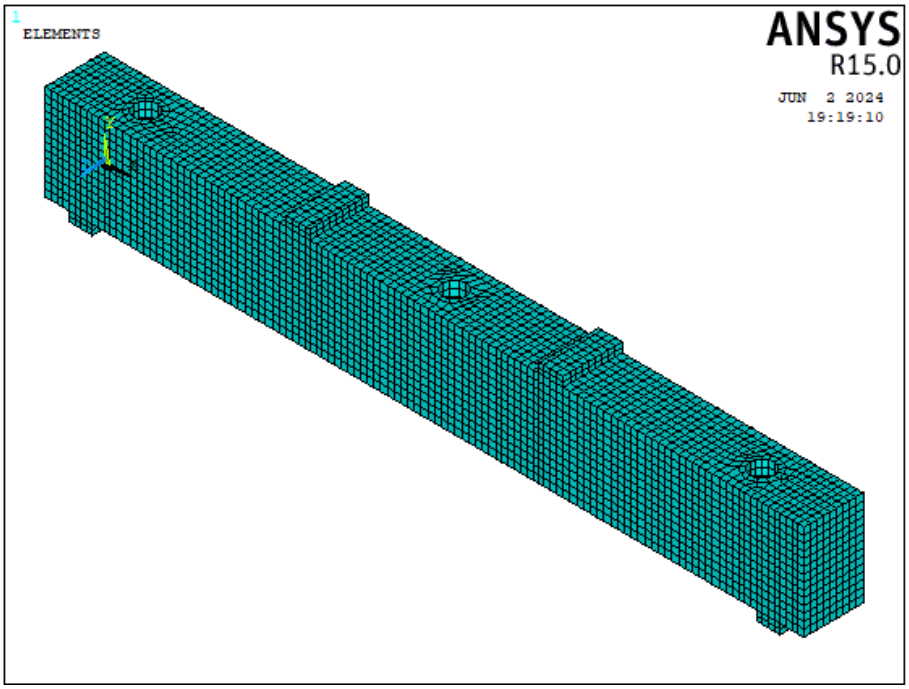

Fig. 18. Concrete, loading and bearing plate idealization.

Table 8. Elastic and plasticity properties of concrete.

State	Parameter	Value
Linear elastic isotropic	Density	2.4×10^{-9} N/mm^3
	Mod. of elasticity	12222.22 MPa
	Poisson's ratio	0.168
Nonlinear	Open shear transfer coefficient	0.2
	closed shear transfer coefficient	0.8
	Uniaxial cracking stress	2.0
	Uniaxial crushing stress	20
	Tensile crack factor	0.6

Table 9. Elastic characteristics of steel bars and metal meshes.

Steel 28/35		Welded mesh		Expanded mesh	
Density		Density		Density	
7.86×10^{-9}		7.86×10^{-9}		7.8×10^{-9}	
Mod. of elasticity	Poisson's ratio	Mod. of elasticity	Poisson's ratio	Mod. of elasticity	Poisson's ratio
205000	0.3	63025.64	0.28	20515.46	0.28
Stress	Strain	Stress	Strain	Stress	Strain
280	0	737.4	0.0117	199	0.0097
350	0.0951	834	0.0588	320	0.0592

6.2. Validation model

A correlative investigation based on the load-deflection response, crack pattern, and failure mode is conducted to verify the numerical model against experimental results. The experimental and numerical results are compared for validation, as shown in Fig. 19. Table 10 presents a comparison between the numerical and experimental failure loads, along with the deflections at the ultimate load of the tested beams. Additionally, the average ratio of the numerical ultimate loads to the experimental failure loads is 1.05, and for deflections at ultimate loads, it is 1.06. This confirms the model's accuracy and indicates a good agreement between the meas-

ured and expected load-deflection curves. Additionally, when comparing the predicted crack patterns of the numerical models in Fig. 20 with those in Fig. 17, there is a good agreement between the predicted crack patterns and those observed in the experimental studies. Consequently, using the structural analysis program ANSYS V.15 to modeling beams non-linear shear behaviors represents the actual behavior of these beams.

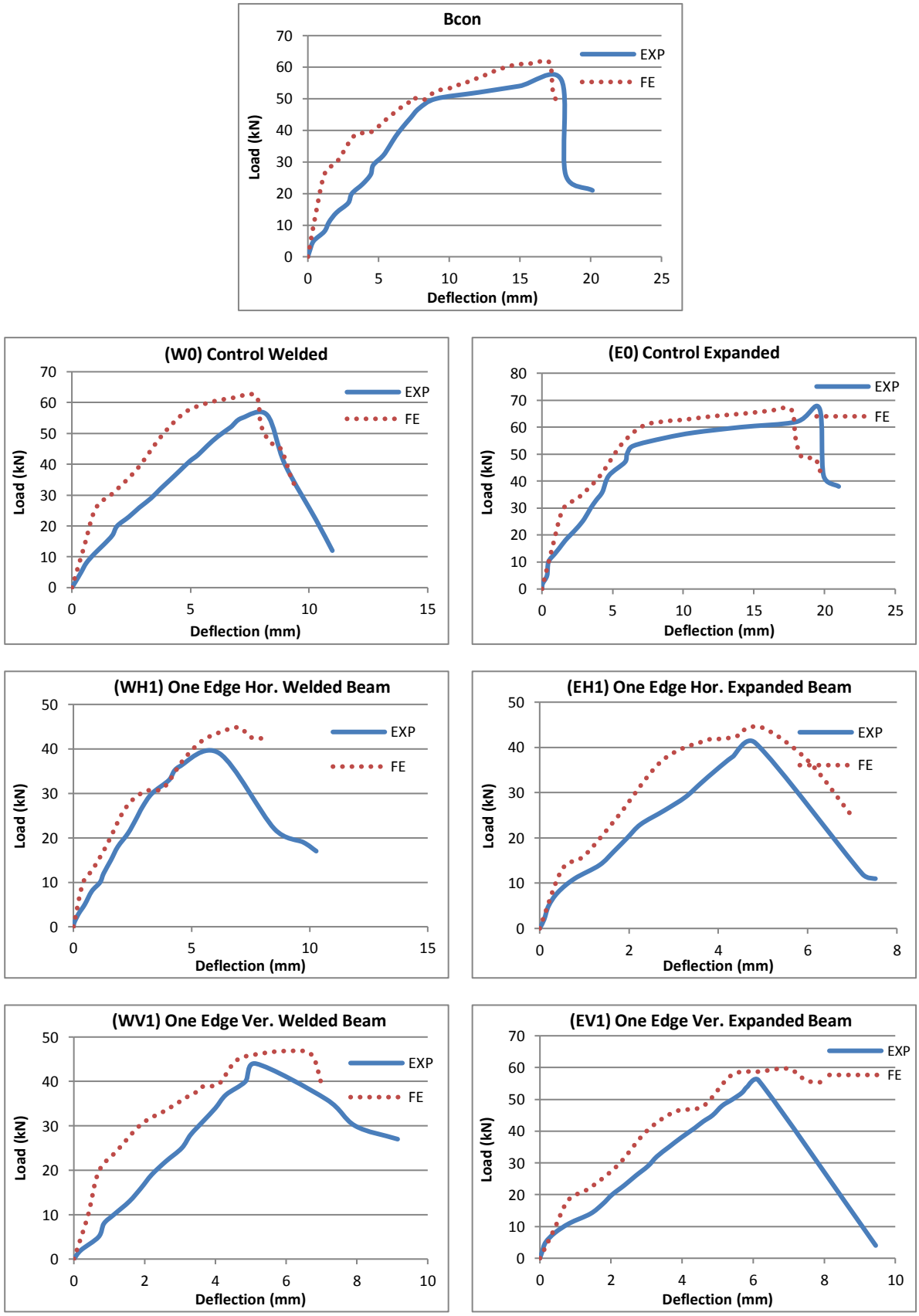

Fig. 19. (continued)

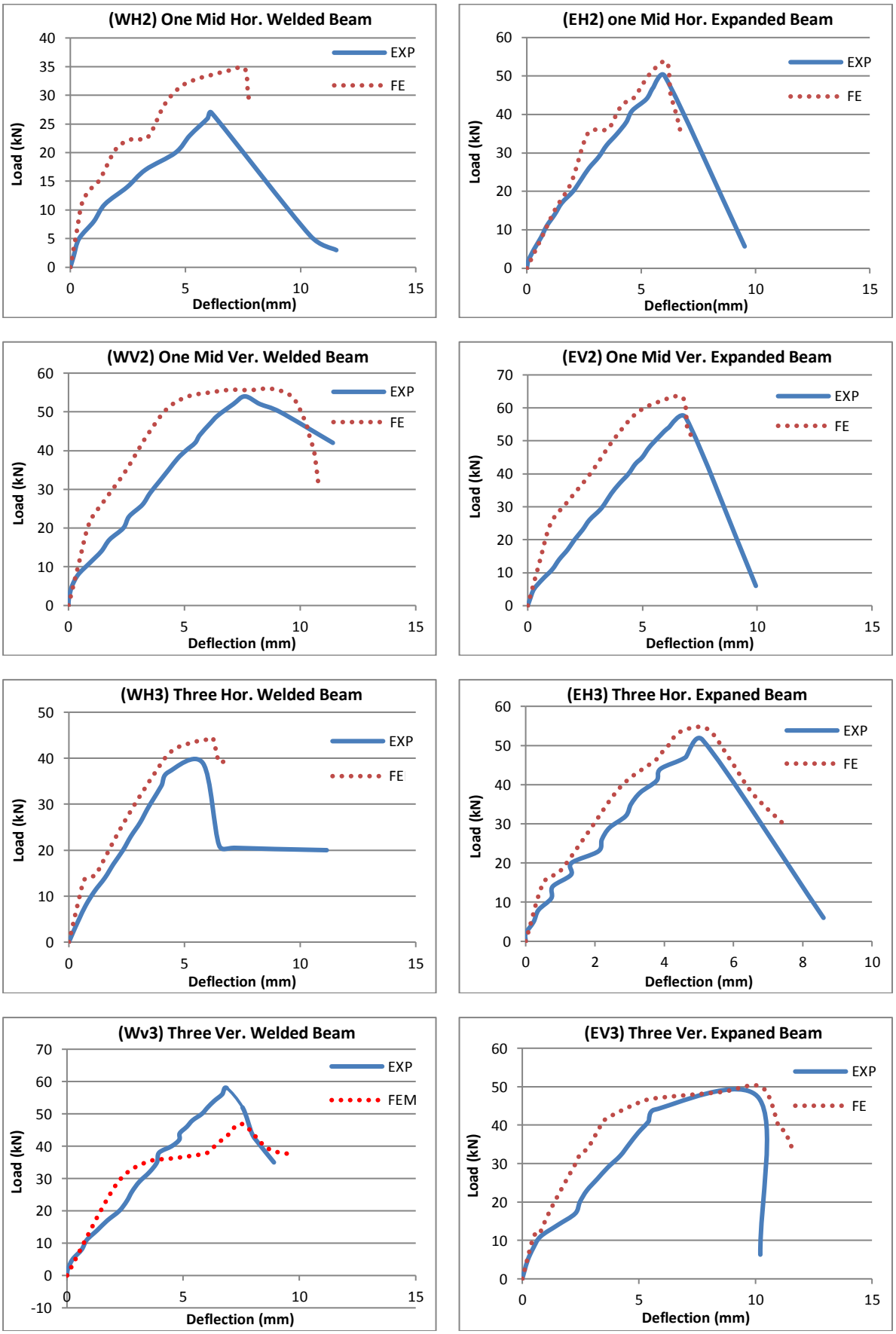

Fig. 19. Experimental and numerical load-deflection curves of the tested beams.

Table 10. Comparison between experimental and numerical results.

		Ultimate load (kN)			Deflection at ultimate load Δf (mm)		
Groups	Beam no.	Numerical	Experimental	Num./Exp.	Numerical	Experimental	Num./Exp.
A (control)	Bcon	61.58	58.80	1.05	17.06	18.02	0.95
B (welded)	W0	62.26	56.70	1.09	7.75	8.23	0.94
	WH1	44.82	41.20	1.08	7.00	6.08	1.15
	WV1	46.83	44.90	1.04	6.00	5.15	1.16
	WH2	34.63	27.70	1.25	7.57	6.12	1.24
	WV2	55.94	55.70	1.01	8.78	8.17	1.07
	WH3	44.32	38.90	1.14	6.23	5.80	1.07
	WV3	46.84	57.388	0.82	7.55	7.21	1.05
C (expanded)	E0	66.59	67.30	0.99	17.63	19.63	0.90
	EH1	44.32	42.60	1.04	5.00	4.96	1.01
	EV1	59.61	57.20	1.04	7.87	6.15	1.27
	EH2	53.69	50.30	1.06	6.11	6.03	1.03
	EV2	63.13	57.60	1.09	6.75	6.89	0.98
	EH3	54.29	51.40	1.05	5.23	5.11	1.02
	E V3	49.84	46.50	1.07	10.28	9.40	1.09
Average				1.05			1.06

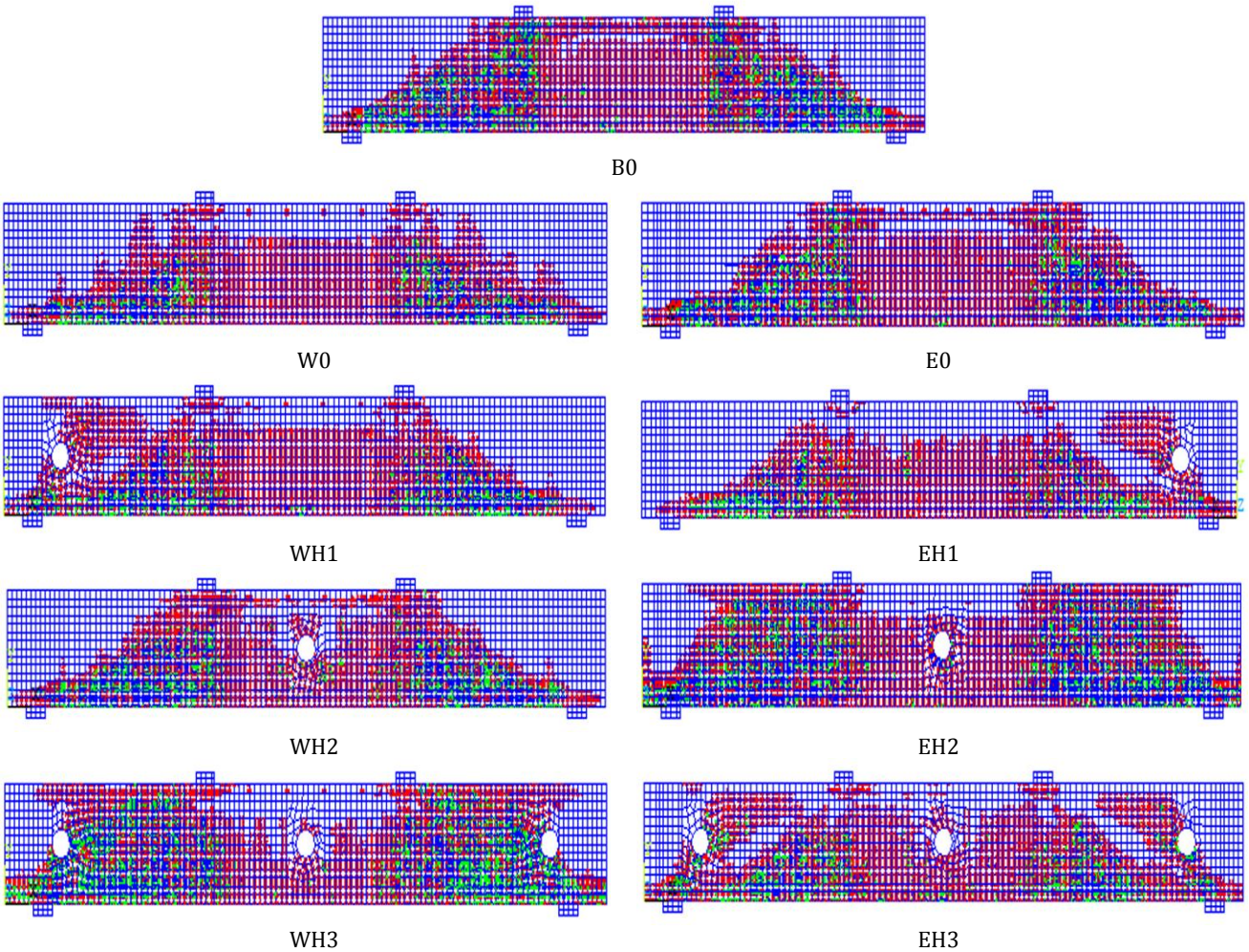

Fig. 20. (continued)

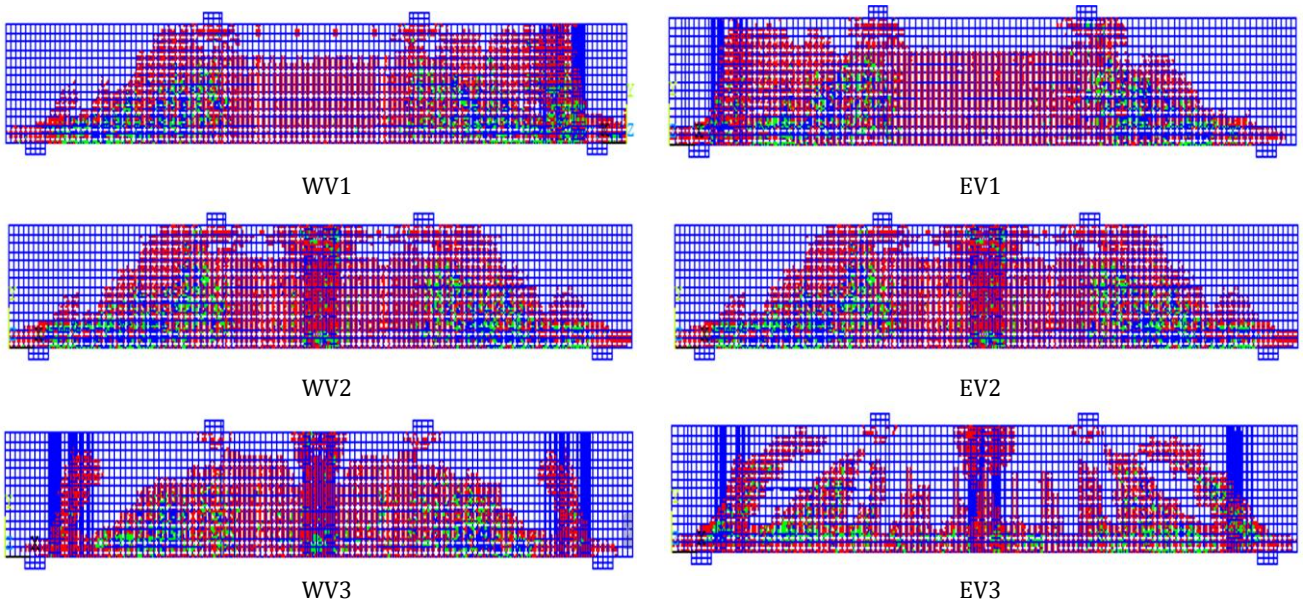

Fig. 20. Numerical crack patterns and failure modes of all tested beams.

7. Conclusions

Here are the conclusions that can be drawn based on the experimental and numerical study investigating the behavior of ferrocement beams with circular openings, within the range of the studied variables:

- The performance of beams is significantly influenced by the type of mesh and the orientation of openings. Horizontal openings reduce the ultimate load more in welded mesh beams, while vertical openings have a greater negative impact on expanded mesh beams. Both types of beams experience reduced deflection with openings, though the extent varies.
- In the Welded Group (B), beams exhibited varying first crack loads and showed a wide range of ultimate load capacities, with some beams demonstrating lower ductility and higher brittleness, which raises concerns about potential brittle failure. These beams also had reduced energy absorption compared to the control, reflecting their diminished ability to handle dynamic loads. Conversely, the Expanded Group (C) showed higher first crack loads and better overall performance, including enhanced ductility and energy absorption, indicating that the expansion process improves both strength and deformation capacity compared to the welded beams.
- In beams with welded steel meshes, both compressive and tensile strains were higher compared to beams with expanded steel mesh. For control beams W0 and E0, the initial cracks were attributed to bending, resulting in a lower first crack load compared to other beams where cracks were a combination of bending and shear due to an increased number of openings, particularly in shear zones. This concentration of stresses around the openings in shear zones contributed to an increased first crack load, attributed to the enhanced shear strength of expanded mesh
- The numerical simulations conducted using ANSYS V.15 demonstrated good agreement with experimental results, accurately predicting load-deflection behavior, crack patterns, and failure modes, validating the use of finite element analysis in studying ferrocement beams with openings.
- The findings suggest that careful consideration must be given to the placement and size of openings in ferrocement beams to minimize the adverse effects on structural performance, and that expanded steel mesh can be a preferable reinforcement option in such scenarios. It is also recommended to study the behavior of ferrocement beams with opening under impact, dynamic loads, and earthquake conditions.

Acknowledgements

This research has previously been presented at the 2nd International Summit on Civil, Structural and Environmental Engineering (ISCSEE2024) held in Florence, Italy, on March 18-20, 2024. Extended version of the research has been submitted to Challenge Journal of Structural Mechanics and has been peer-reviewed prior to the publication.

The authors would like to thank to the technical support from the construction material laboratory of the Faculty of Engineering, Menoufia University, Egypt because of their help.

Funding

The authors received no financial support for the research, authorship, and/or publication of this manuscript.

Conflict of Interest

The authors declared no potential conflicts of interest with respect to the research, authorship, and/or publication of this manuscript.

Author Contributions

All of the authors made substantial contributions to conception and design, or acquisition of data, or analysis and interpretation of data; were involved in drafting the manuscript or revising it critically for important intellectual content; and gave final approval of the version to be published.

Data Availability

The datasets created and/or analyzed during the current study are not publicly available, but are available from the corresponding author upon reasonable request.

REFERENCES

Abou-Zeid MN (2002). Recycled aggregates concrete: advancement and future. *Proceedings of the Workshop on Expansive Reactions, Admixtures and Blended Cement in Relation to Concrete Quality*, Helwan University, Egypt, 26-27.

ANSYS V.15 (2015). Manual Set. ANSYS Inc., Canonsburg, PA, US. https://forum.ansys.com/uploads/846/SCJEU0NN8IHX.pdf

E.S.S. 262 (2011). Egyptian standard specifications for steel bars. Egyptian Standards Specification, Cairo, Egypt.

E.S.S. 1109 (2008). Egyptian standard specifications: aggregates for concrete. Egyptian Standards Specification, Cairo, Egypt.

E.S.S. 4756-11 (2013). Physical and mechanical properties examination of cement, Part 1. Egyptian Standards Specification, Cairo, Egypt.

Hekal GM, Elshaboury AMM, Shaheen YBI (2024). The impact of openings on ferrocement I-beams: a study on metallic and non-metallic mesh reinforcement. *Challenge Journal of Concrete Research Letters*, 15(2), 30-46.

Rashwan MS, Abourizk S (1997). The properties of recycled concrete. *Concrete International*, 19(7), 56-60.

Shaheen YBI, Hassanen M (2011). Structural Behavior of reinforced concrete columns reinforced with various materials. *Proceedings of 18th International Conference on Composite Materials*, Jeiu Island, South Korea, W04-5.

Shaheen YBI, Essam AE (2017). Structural behavior of ferrocement channels slabs for low-cost housing. *Challenge Journal of Concrete Research Letters*, 8(2), 48-64.

Shaheen YBI, Hala MA (2017). Structural behavior for rehabilitation ferrocement plates previously damaged by impact loads. *Case Studies in Construction Materials*, 6(1), 72-90.

Shaheen YBI, Etman ZA, Seyam AM (2022). Structural characteristics of lightweight ferrocement walls with various types of core materials and mesh reinforcement. *Current Journal of Applied Science and Technology*, 41(18), 15-45.

Shaheen YBI, Etman ZA, Kandil D (2023a). Performance of light weight ferrocement composite walls. *Challenge Journal of Concrete Research Letters*, 14(3), 69-88.

Shaheen YBI, Etman ZA, Elhosine NK (2023b). Flexural behavior of light-weight ferrocement composite beams. *Advanced Engineering Technology and Application,* 2, 13-23.